Pergamon

Int. J. Heat Mass Transfer. Vol. 38, No. 15, pp. 2893–2903, 1995

0017–9310/95 $9.50+0.00

0017–9310(95)00031–3

Laminar and turbulent free convection in vertical cylinders with internal heat generation†

M. HOLZBECHER and A. STEIFF‡

Department of Chemical Engineering, Dortmund University, P.O. Box 400 400, 44221 Dortmund, Germany

(*Received* 20 *July* 1994)

Abstract—Natural convection flow in internally heated vertical cylinders is investigated experimentally and numerically. Experimental facilities restricted the Rayleigh number range from 3×10^{10} to 1×10^{14}, covering the laminar boundary layer regime and the first transitions to turbulent flow. Laminar and turbulent natural convection in cavities differ significantly with regard to the influence of boundary conditions. For the numerically calculating turbulent flow, several low-Reynolds number k–ε models are tested. They all fail to correctly predict experimentally observed laminar–turbulent transitions.

1. INTRODUCTION

A variety of expressions and correlations of experimental and numerical data have been derived for predicting natural convection heat transfer.

Over the past two decades, even vertical enclosures have been the topic of much research. The standard case of vertical enclosures consists of a rectangular cavity with two side walls on different temperatures; the remaining surfaces are adiabatic (hot wall–cold wall case) [1–14].

Natural convection with volumetric heating has received much less attention. Boundary conditions differ widely. Therefore, it can be said no standard case exists. The favorite geometries are cylinders to which the present paper is restricted [15–21] but also rectangular cavities [22–27]. The horizontal boundaries are partly isotherm partly adiabatic. In the theoretical studies, vertical boundaries are mostly isotherm while in experiments wall temperatures depend on the conjugate heat transfer. Furthermore, the varying aspect ratio makes the comparison between different studies more difficult.

The present study is motivated by safety problems regarding the cooling of exothermal chemical reactions and radioactive processes. For these cases, confidential correlations are essential. It is therefore necessary to clarify the influence of variant boundary conditions on laminar and turbulent natural convection flows.

It seems appropriate to discuss these two cases separately because the calculation of turbulent flow requires the inclusion of turbulence models. Natural convection in enclosures is characterized by low velocities and regions of recirculation. To meet these conditions, a more sophisticated turbulence model than the widespread ordinary k–ε model is necessary. Considering previous work the choice fell on low-Reynolds number k–ε models.

All experiments and numerical simulations presented in this paper were performed with water or, respectively, with the physical properties of water.

2. EXPERIMENTAL APPARATUS AND INSTRUMENTATION

For the experimental part of this study, two vertical cylindrical glass vessels with diameters of 0.29 m ($H = 0.37$ m, $t \approx 5$ mm) and 0.49 m ($H = 0.75$ m, $t \approx 9.5$ mm) were used. They were surrounded by thick plexiglas cylinders leaving an annulus for forced convection water cooling (Fig. 1(a)).

On both sides of the glass cylinders several thermocouple probes were embedded to detect inner and outer wall temperature distributions. A traversing mechanism for three thermocouple probes was installed to measure the temperature field in the fluid. All thermocouples were insulated electrically from the test fluid.

The very low flow velocities could be determined with great accuracy by a LDA (Laser Doppler Anemometer) fibre optic system.

While the vessel bottom was isolated, evaporation was possible at the free fluid surface. This evaporation was detected by a very precise measurement of level changes during steady state conditions. Steady state was normally reached after 3–5 h depending on cylinder size and power input.

† Dedicated to the 60th birthday of Professor Dr.-Ing. Paul-Michael Weinspach.

‡ Author to whom correspondence should be addressed.

NOMENCLATURE

A	area
c	constant; special low-Reynolds numbermodel constant: c_{1e}, c_{2e}, c_{3e}
c_p	heat capacity
D	vessel diameter
E	extra term of the JL and LS low-Reynolds number k–ε model
f_2, f_k	functional expression of low-Reynolds number turbulence models modifying c_{2e}, c_μ
H	vessel height
h	enthalpy
IZ	number of grid points in z-direction
k	turbulent energy
n	coordinate normal to the wall
NR	last grid point in r-direction
p	pressure
r	radial coordinate
S	source term
T	temperature
T_b	core temperature at the bottom
T_c, T_{cm}	core temperature, mean value
T_i, T_{im}	temperature at the inner surface of the glass cylinder, mean value
T_{max}	maximal temperature
T_{min}	minimal temperature
T_o	temperature at outer surface of glass cylinder
T_t	core temperature at the top
ΔT_v	vertical temperature difference $T_t - T_b$
t	thickness of the solid wall
v	velocity in r-direction
w	velocity in z-direction
z	vertical coordinate
Gr	Grashof number
Ra	Rayleigh number, $Ra = Pr \cdot Gr$
Ra_v	Rayleigh number based on the vertical temperature difference ΔT_v
Re	Reynolds number uD/v
Re_t	turbulent Reynolds number
Nu	Nusselt number
WR	wall resistance number.

Greek symbols

ε	dissipation of turbulent energy
ε_w	dissipation of turbulent energy at wall
λ	thermal conductivity
ν	kinematic viscosity
ν_t	turbulent viscosity
ρ	density
σ_t	turbulent Prandtl number

Joule heating by an alternating current (50 Hz), passing vertically through the fluid, provided an almost uniformly distributed volumetric energy source. For this, a stainless steel plate fixed at the bottom served as the lower electrode. The other electrode consisted of a stainless steel wire trellis, fixed one centimeter underneath the fluid surface. For the smaller cylinder, a maximum voltage of 220 V and a maximum power input of 850 W could be reached. The values for the larger cylinder were 400 V and 4500 W.

The experiments in the smaller cylinder showed

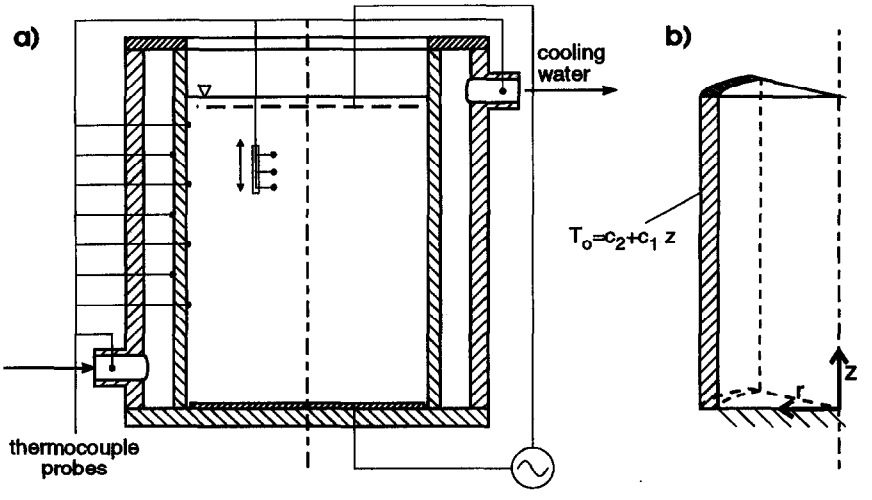

Fig. 1. (a) Schematic illustration of the experimental set-up. (b) Geometry and coordinate system.

laminar flow behaviour with a maximum Rayleigh number of 1×10^{13} while, in the larger one, it was additionally possible to study turbulent flow characteristics ($Ra_{max} = 1 \times 10^{14}$).

3. NUMERICAL PROCEDURE

Mathematically, the problem of buoyancy-driven flow is described by a set of coupled non-linear partial differential equations in which this buoyancy dictates flow patterns.

Because of the axisymmetrical flow the three-dimensional (3D) flow situation reduces to a 2D problem [Fig. 1(b)] described by the following set of equations for the single-phase incompressible fluid.

3.1. *Continuity*

$$\frac{\delta w}{\delta z} + \frac{1}{r}\frac{\delta}{\delta r}(rv) = 0 \tag{1}$$

3.2. z-*Momentum*

$$\frac{\delta}{\delta z}w^2 + \frac{1}{r}\frac{\delta}{\delta r}(rvw) = -\frac{1}{\rho}\frac{\delta p}{\delta z} + \nu_{eff}\frac{\delta^2 w}{\delta z^2} + \frac{\nu_{eff}}{r}\frac{\delta}{\delta r}\left(r\frac{\delta w}{\delta r}\right) + g\beta\frac{1}{c_p}(h - h_{ref}) \tag{2}$$

3.3. r-*Momentum*

$$\frac{\delta}{\delta z}(wv) + \frac{1}{r}\frac{\delta}{\delta r}(rv^2) = -\frac{1}{\rho}\frac{\delta p}{\delta r} + \nu_{eff}\frac{\delta^2 v}{\delta z^2} + \frac{\nu_{eff}}{r}\frac{\delta}{\delta r}\left(r\frac{\delta v}{\delta r}\right) - 2\nu_{eff}\frac{v}{r^2} \tag{3}$$

3.4. *Energy equation*

$$\frac{\delta}{\delta z}(\rho wh) + \frac{1}{r}\frac{\delta}{\delta r}(\rho rvh) = \frac{\lambda_{eff}}{c_p}\frac{\delta^2 h}{\delta z^2} + \frac{1}{r}\frac{\lambda_{eff}}{c_p}\frac{\delta}{\delta r}\left(r\frac{\delta h}{\delta r}\right) + S_h(r, z, h) \tag{4}$$

with $\nu_{eff} = \nu + \nu_t$ and $\lambda_{eff} = \lambda + \nu_t/\sigma_t$.

Boundary conditions:

$$r = 0: \quad \frac{\delta h}{\delta r} = \frac{\delta v}{\delta r} = \frac{\delta w}{\delta r} = 0$$

$$r = R: \quad w = 0;\ \frac{\delta h}{\delta r} = \frac{\delta v}{\delta r} = 0$$

$$z = 0: \quad v = 0;\ \frac{\delta h}{\delta z} = \frac{\delta w}{\delta z} = 0$$

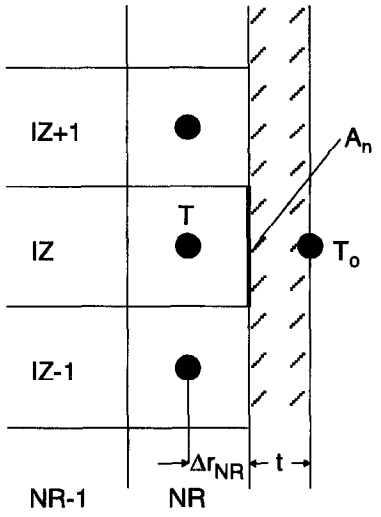

FIG. 2. Simplified consideration of the conjugate heat transfer in the numerical calculation procedure.

$$z = H: \quad \frac{\delta h}{\delta z} = \frac{\delta v}{\delta z} = \frac{\delta w}{\delta z} = 0.$$

All physical properties are evaluated at the mean temperature T_{ref} and are assumed to be constant. The temperature dependence of the density is only considered in the last expression on the right hand side of the z-momentum equation (Boussinesq approximation).

To describe the conjugate heat transfer at the inner side of the glass cylinder, a special source term S_q is introduced for the last grid point in r-direction, including the 1D heat conduction in the glass wall (Fig. 2):

$$S_q(NY, IZ) = \left(\frac{\Delta y_{NY}}{\lambda} + \frac{t}{\lambda_W}\right)^{-1} \times A_n(NY, IZ)(T_0 - T). \tag{5}$$

For small t/R ratios, realistic results can be expected with this simplification [28].

To face the great gradients of temperature and velocity in the near wall region, the grid in r-direction is extremely nonuniform. The same applies in a moderate way to the z-direction.

The above equations are solved by the finite-domain program PHOENICS, Cham, England. Hybrid differencing is used in the convective terms. For the pressure–momentum link, the 'SIMPLEST' practice is followed. Further details may be found in [29].

4. PROOF OF THE NUMERICAL METHOD FOR THE LAMINAR CASE

The numerical method was tested in two different ways. At first, a pure numerical test with a consequent grid refinement was performed.

Figure 3 demonstrates the dependence of the overall

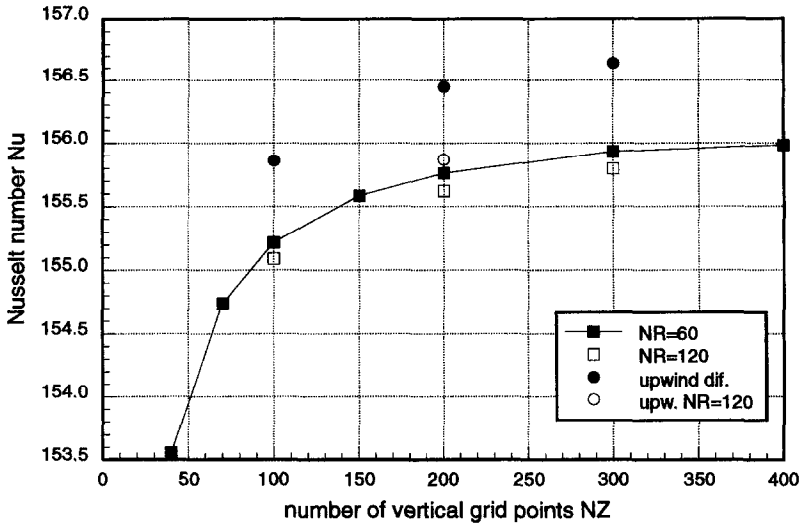

Fig. 3. Dependence of the overall Nusselt number on the number of vertical grid points.

Nusselt number on the number of grid points in z-direction. It is obvious that for a very high cell number a grid independent solution exists. Furthermore, the superiority of the hybrid scheme is demonstrated.

As a compromise of accuracy and calculation speed, 100 grid points were chosen for the vertical direction and 60 points for the horizontal direction. A comparison between numerical and experimental results is presented in Fig. 4. For the calculation, an assumption about the temperature distribution at the outer surface of the glass cylinder is necessary, depicted in the picture as a pointed line.

In addition, the inhomogeneous heat source distribution of the experiment is taken into account by the calculation. That means, that in the calculation no heat is released above the upper electrode, and the electrical conductivity of the fluid changes in line with vertical temperature stratification. As a simplification, current density is assumed to be constant everywhere which is not exactly true for the near wall region.

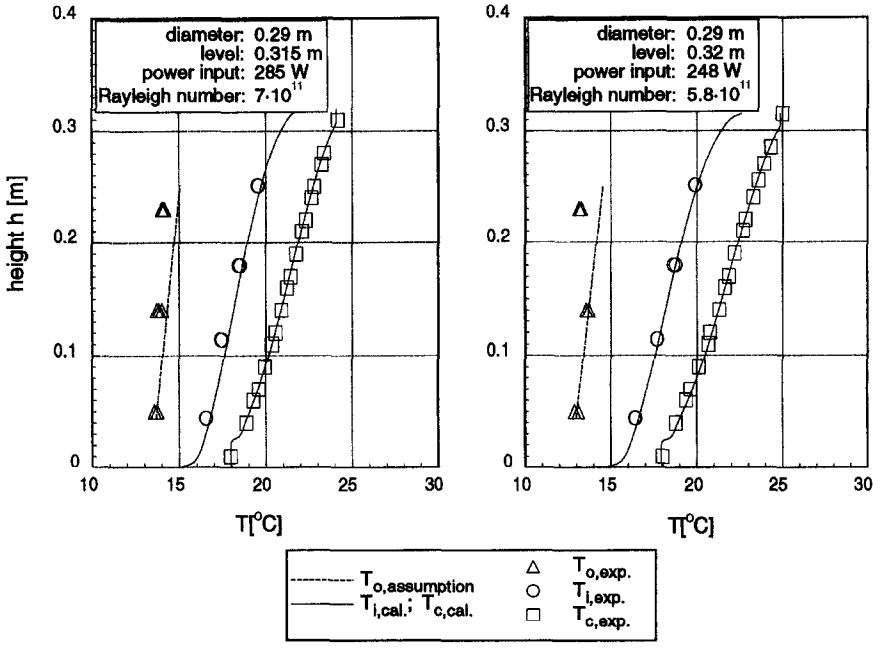

Fig. 4. Comparison between numerical and experimental vertical temperature profiles.

Nevertheless, there is a good correspondence of numerical and experimental results.

Equal comparison studies for several experiments, including also velocity profiles, always show similar results, thus confirming the calculation procedure.

5. HEAT TRANSFER CORRELATIONS FOR THE LAMINAR CASE

The numerical procedure validated in the last paragraph was first used to determine the heat transfer correlation for the ideal case which means a cylinder with adiabatic horizontal walls, isothermal vertical walls and a completely homogeneous heat source distribution

$$Nu = 0.576\, Ra^{0.2024}(H/D)^{-0.186} \tag{6}$$

for $3 \times 10^{10} < Ra < 1 \times 10^{13}$.

The influence of the aspect ratio agrees with data of Kulacki and Richards ($(H/D)^{-0.21}$) [26] who examined a similar case. It also corresponds with data collected from the hot wall–cold wall case without internal heat sources.

It has been already mentioned that calculations normally proceed from isothermal side walls while in experiments this ideal condition cannot be realized. Therefore, the influence of temperature gradients at the inner wall has to be quantified. In the present paper two types of boundary conditions were examined.

First, a linear temperature gradient was chosen for the inner wall. With a rising positive temperature gradient, the overall Nusselt number also increases. A negative temperature gradient reduces the mean heat transfer rate. For quantitative data refer to [30]. The second case starts with an isothermal outer wall and a wall thickness of zero, which is equivalent to the isothermal case. Then the wall thickness t, or more precisely the value t/λ_W, is raised, resulting in a wall temperature distribution which is determined by the conjugate heat transfer. This case corresponds to most of the experimental facilities.

To receive a correlation not depending on cylinder size, fluid properties and power input, a new dimensionless number has been introduced

$$WR = Ra^{0.2024}\frac{s/\lambda_W}{R/\lambda}. \tag{7}$$

The relative increase of the mean Nusselt number with rising values of WR can be seen in Fig. 5. This relation will help to quantify the influence of nonisothermal sidewalls due to conjugate heat transfer and gives, therefore, a good explanation for the scatter of existing heat transfer data. Thick walls with a low thermal conductivity and relatively high Rayleigh numbers result in significantly higher overall Nusselt numbers.

For the experiment presented in the left part of Fig. 4, the wall resistance number WR is 4.6. This means that the Nusselt number is about 12% higher than for the corresponding case with the isothermal inner wall. The slight temperature gradient at the outer surface strengthens this effect. Of course, it is impossible to raise the mean heat transfer coefficient to infinity by increasing the positive temperature gradient at the inner wall. The maximum obtainable improvement is about 55%.

An analysis of the whole simulation data shows that an increase of Nusselt number is always correlated with an increase of the vertical temperature difference divided by the aspect ratio

$$\Delta T_v = (T_t - T_b)/(H/D) \tag{8}$$

A definition of the Rayleigh number based on ΔT_v gives

$$Ra_v = g\beta\Delta T_v D^3/(va) \tag{9}$$

which is almost identical with the definition of Smith and Hammit [22] who substituted the maximum temperature difference $T_{max} - T_{min}$ for the characteristic temperature difference.

Figure 6 shows a plot of Nusselt number over Ra_v which turned out to be independent of the cylinder size, aspect ratios, fluid properties and also of the temperature distribution at the inner side wall. Especially the last point does not agree with the result of Smith and Hammit. The constant of their equation differs with the temperature gradient at the inner wall. However, their exponent of 0.25 is identical to our expression

$$Nu = 0.776 Ra_v^{0.246} \tag{10}$$

It can be assumed that equation (10) will not be valid as soon as the flow becomes turbulent because turbulence reduces the temperature gradients in each direction. An increase of the Nusselt number due to turbulence is always coupled with a decrease of the vertical temperature difference ΔT_v.

Experiments in the bigger cylinder show turbulent behaviour. As expected, the variation of the aspect ratio indicates no influence on the Nusselt number which contradicts the laminar case. For further investigations, numerical results based on the introduction of turbulence models are necessary. This topic will be discussed in the next section.

6. TURBULENCE MODELING

For cylinder geometries with internal heat sources, no turbulent numerical calculation results are available. But there are a lot of investigations for the hot wall–cold wall configuration [8, 9, 11, 12, 31–35] and also for natural convection at a heated plate [36, 37].

The work of Henkes and Hoogendoorn [35, 37] is especially remarkable because they compare different low-Reynolds number k–ε models, extended by special terms integrating the influence of buoyancy. They recommend the models of Jones and Launder (JL) [38], Lam and Bremhorst (LB) [39] and Chien [40]. The

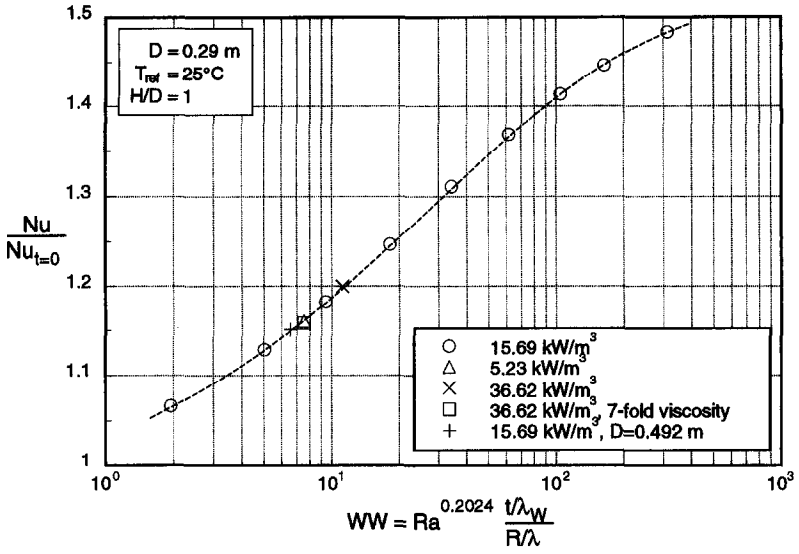

Fig. 5. Relative increase of the overall heat transfer depending on WR.

LB model and the Chien model are mainly adjusted to the near wall behaviour of the turbulent fluid flow. For natural convection in an enclosure the turbulence intensity is normally also very low in the core. Therefore, the low-Reynolds number extensions must also be effective in this flow region. Test calculations with the model of LB and Chien confirm these difficulties. The same statement can be made about the more recently published low-Reynolds number model of Abe *et al.* [41]. Davidson [33] also criticizes that the f_k function of the LB model includes the wall distance which is not appropriate to predict low-Reynolds number flow in free recirculating flows. They substitute this term by the f_k function of JL. This procedure seems very dubious because each model should be treated as a unit.

In the present study, the model of Launder and Sharma (LS) [42] is used, which is a slightly changed version of the JL model.

The LS boundary condition of ε_w equals zero requires the introduction of an additional term D in the k equation. To circumvent this inconvenient approximation the alternative boundary condition $(d\varepsilon/dn) = 0$ at walls tested by Patel *et al.* [43] is used in the present work. Besides, the LS model was further modified to account for buoyancy effects.

A complete comparison of the original LS model and the model used in this paper is shown in Table 1.

7. COMPARING EXPERIMENTAL AND NUMERICAL RESULTS

A numerical simulation of the experiments of the greater cylinder leads, independently of the power

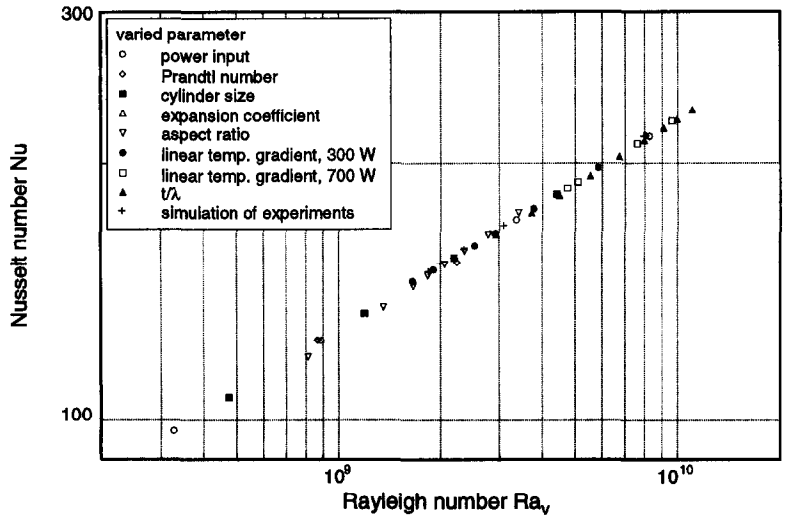

Fig. 6. Overall heat transfer depending on Ra_v.

Table 1. Comparison between the original LS model and the modified model

Model	c_k	c_{1e}	c_{2e}	c_{3e}	σ_k	σ_e	σ_t	f_k
LS	0.09	1.44	1.92	—	1.0	1.3	1.0	$\exp\frac{-3.4}{(1+Re_t/50)^2}$
Modified	0.09	1.44	1.92	0.7	1.0	1.3	1.0	$\exp\frac{-3.4}{(1+Re_t/50)^2}$

Model	f_1	f_2	E	D
LS	1.0	$1-0.3\exp(-Re_t^2)$	$2\nu\nu_t\left(\frac{\delta^2 v}{\delta z^2}+\frac{\delta^2 w}{\delta r^2}\right)^2$	$-2\nu\left(\frac{\delta\sqrt{k}}{\delta y}\right)^2$
Modified	1.0	$1-0.3\exp(-Re_t^2)$	$c\cdot 2\nu\nu_t\left(\frac{\delta^2 v}{\delta z^2}+\frac{\delta^2 w}{\delta r^2}\right)^2$	

Model	ε_w Boundary condition	Buoyancy term	Additional source term
LS	0	—	—
Modified	$\left(\frac{\delta\varepsilon}{\delta r}\right)_{r=R}=0\ \left(\frac{\delta\varepsilon}{\delta z}\right)_{z=0,H}=0$	$G, c_{3e}\cdot\frac{\varepsilon}{k}G$	in the k equation for $Re_t<40$ and $Re>4000$

input and aspect ratio, to laminar solutions. Similar problems with low-Reynolds number models are described by Nobile *et al.* [13] and Henkes *et al.* [35]. They always occur for moderate Rayleigh numbers and aspect ratios.

In contrast, the experimental data demonstrate significant turbulent behaviour. How could this discrepancy be explained?

Due to very low velocities in the core and thermal stratification, the upstreaming fluid undergoes a complete relaminarization. Turbulence production takes place only in the small near wall region where cooled fluid streams downward. But the production term P_k of the k equation is reduced by the f_k function which can be extremely small for neglectable turbulence intensity. This means the growth of turbulent energy is prevented as long as the value of this variable is very low. Therefore, the laminar–turbulent transition is retarded in low-Reynolds number models.

In the present study an empirical additional source term $\nu_t cP$ is introduced to get realistic turbulent behaviour. For control volumes with relative high velocities or Reynolds numbers ($Re > 4000$) but neglectable turbulent Reynolds numbers the source term of the k equation is increased by a maximum of 60%.

$$\nu_t P + \nu_t cP$$

$$P=\left(\frac{\delta v}{\delta z}+\frac{\delta w}{\delta r}\right)^2+2\left(\left(\frac{\delta v}{\delta r}\right)^2+\left(\frac{\delta w}{\delta z}\right)^2+\left(\frac{v}{r}\right)^2\right) \qquad (11)$$

$c = 0.6$ if $Re_t < 20$, $c = 0$ if $Re_t > 40$.

As soon as the turbulence production starts, the turbulent Reynolds number goes up and the additional source term vanishes. For this reason, the additional source term is restricted to very small regions. Beyond these regions, the model remains unchanged.

Figures 7 and 8 show a comparison of experimental and numerical radial velocity and vertical temperature profiles with the special LS extra term E used as a parameter. This term is disregarded by most publications [11, 12, 31, 33, 36]. Only Henkes and Hoogendoorn [37] emphasize the importance of this term for the LS model. They demonstrate that ignoring this empirical term leads to a significant overprediction of the mean Nusselt number.

For the special case regarded in this paper, an evaluation of E of about 40% gives the best agreement with experimental data, velocity and temperature profiles. It is not surprising that the term E differs according to the flow problem because of its pure empirical origin. Another disadvantage is the fact that in contrast to low-Reynolds number extensions the term E does not vanish with growing turbulence intensity in order to secure the transition to the standard k–ε model. This requires a special criterion for the range of validity for the term E. Experimental facilities of our present study limited the maximum Rayleigh number to 1×10^{14}. Therefore, all experiments took place in the very low-Reynolds number regime. A criterion for the transition to the high-Reynolds number regime is not necessary.

For the low-Reynolds number regime, three main results concerning turbulence modeling should be pointed out:

(1) In the numerical simulation of the experiments the laminar–turbulent transition does not occur unless an additional source term is added. Otherwise the LS-model could not predict the development of turbulence correctly..

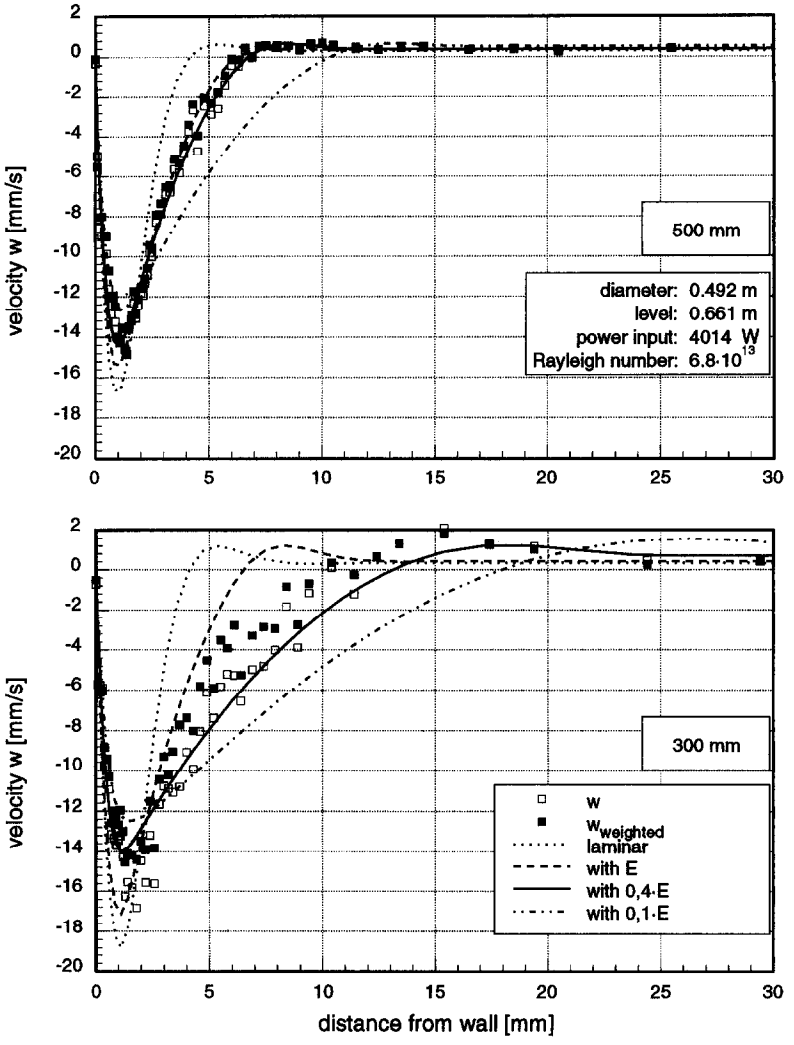

Fig. 7. Numerical and experimental radial velocity profiles.

(2) The empirical extra term E in the ε equation cannot be neglected but has to be weighted to improve the agreement between numerical and experimental results.

(3) In contrast to the extra term E, other empirical constants like c_{3e} are completely insignificant. This statement seems at first astonishing since the importance of the constant c_{3e} is emphasized by several authors.

As shown by (1)–(3), much work is still needed to receive more general low-Reynolds number models. The application of the existing models to the case of natural convection in a cooled cylinder with internal heat generation failed for all tested models. The LS model was the only model which showed realistic results after introducing an additional source term to increase turbulent energy production.

Of course, this additional source term shows some weak points, for example, the empirical determination of the Reynolds number condition: if $Re > 4000$ then....

On the other hand, a fixed transition point depending on the Rayleigh or Grashof number should be avoided. The latter was pursued by Henkes *et al.* [44] who introduced a special amount of turbulent kinetic energy at $Gr = 2 \times 10^9$ to obtain a transition to the turbulent solution.

All the simulations of the low-Reynolds number turbulence flow presented in the next section are realized with the modified LS model.

8. COMPARING LAMINAR AND TURBULENT NATURAL CONVECTION FLOWS

The results of three numerical studies ($Ra = 5 \times 10^{13}$, power input completely homogeneous), differing in aspect ratio and wall thickness, are presented in Table 2. At first the flow was treated laminar. Then the turbulence model was switched on. As expected, the overall Nusselt number goes up while the vertical temperature difference is reduced indicating that equation (10) does not hold any longer.

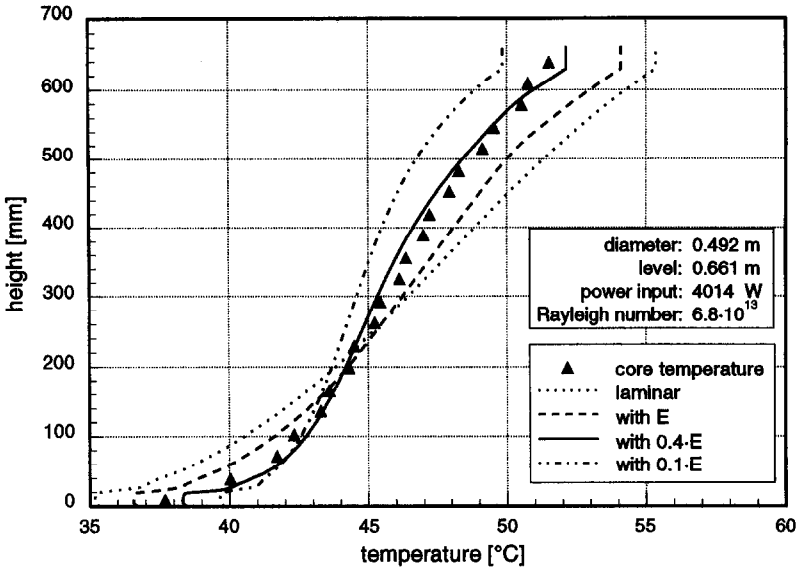

Fig. 8. Numerical and experimental vertical core temperature distributions (T_c = const. (9°C).

$$\bar{u} = \sum_{i=1}^{N} u_i/N\,; \quad \bar{u}_{\text{weighted}} = \sum_{i=1}^{N} u_i\tau_i \Big/ \sum_{i=1}^{N} \tau_i\,.$$

Table 2. Numerical simulations demonstrating the influence of the boundary conditions on Nusselt number and turbulent intensity

H/D	t [mm]	Calculation	$T_t - T_b$ [°C]	$T_{cm} - T_{im}$ [°C]	Ra_v [10^{10}]	Nu	Nu using equation (6) and Fig. 5	Nu using equation (10)
1.5	9.6	laminar	32.3351	8.2294	8.5946	376.42	379.70	379.91
1.5	0	laminar	14.9801	9.8864	3.9817	313.33	315.70	314.40
1	0	laminar	13.4039	9.1321	5.3441	339.21	340.43	338.0
							k_{max} 10^{-6} m^2 s^{-2}	$\nu_{t,max}$ 10^{-6} m^2 s^{-1}
1.5	9.6	turbulent	27.8977	8.0701	7.4151	404.83	9.88	0.876
1.5	0	turbulent	10.7105	8.0829	2.8468	383.25	21	9.96
1	0	turbulent	10.5738	8.2294	4.2157	383.85	16	4.02

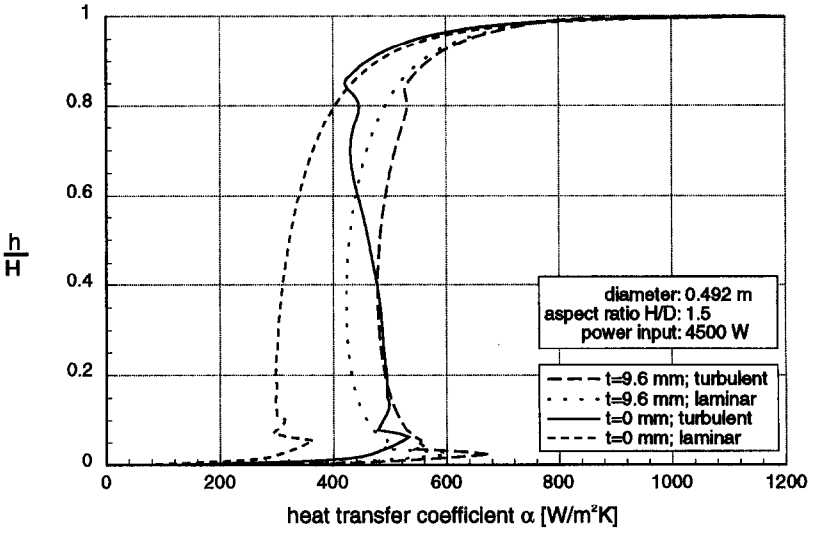

Fig. 9. Laminar and turbulent local heat transfer.

The influence of the wall thickness diminishes in the same way as the influence of the aspect ratio. It should be stressed that the degree of turbulence is very low and depends strongly on boundary conditions. The maximum turbulent viscosity is less than 15 times the laminar one.

Obviously, the experimental set-up suppresses turbulence by the existence of thick glass walls and, respectively, high positive temperature gradients. This fact is illustrated by Fig. 9.

On the other hand, the inhomogeneous heat source distribution increases turbulence production. For the simulated experiment illustrated in Figs. 7 and 8, the assumption of a homogeneous heat source distribution instead of the inhomogeneous distribution existing in the experiment leads to a reduction of turbulent viscosity by more than a factor 3. It is difficult to prove these results experimentally in the present study as heat source distribution and wall thickness cannot be changed significantly. All the same, three points can be summarized:

(1) Turbulence intensity is strongly affected by boundary conditions.

(2) On the other hand, these conditions lose their influence on the overall Nusselt number.

(3) Turbulence intensifies the heat transfer rate in all cases that were considered. Hence the assumption of laminar flow is always a safe estimate.

REFERENCES

1. R. K. MacGregor and A. F. Emery, Free convection through vertical plane layers—moderate and high Prandtl number fluids, *ASME J. Heat Transfer C.*, 391–403 (1969).
2. S. Ostrach, Natural convection in enclosures, *Adv. Heat Transfer* **8**, 161–227 (1972).
3. C. Taylor and A. Z. Ijam, A finite element numerical solution of natural convection in enclosed cavities, *Comput. Meth. Appl. Mech. Engng* **19**, 429–446 (1979).
4. G. H. Cowan, P. E. Lovegrove, and G. L. Quarini, Turbulent natural convection heat transfer in vertical single water-filled cavities, *Proceedings of International Heat Transfer Conference*, Vol. 2, pp. 195–203 (1982).
5. B. Gilly, B. Roux and P. Bontoux, Influence of thermal wall conditions on the natural convection in heated cavities, *Numerical Methods in Heat Transfer*, Vol. 2, Chap. 8, pp. 205–225 (1983).
6. G. de Vahl Davis and I. P. Jones, Natural convection in a square cavity: a comparison exercise, *Int. J. Numer. Meth. Fluids* **3**, 227–248 (1983).
7. G. de Vahl Davis and I. P. Jones, Natural convection of air in a square cavity: a bench mark numerical solution, *Int. J. Numer. Meth. Fluids* **3**, 249–264 (1983).
8. N. C. Markatos and K. A. Pericleous, Laminar and turbulent natural convection in an enclosed cavity, *Int. J. Heat Mass Transfer* **27**, 755–772 (1984).
9. H. Ozoe, A. Mouri, M. Ohmuro, S. W. Churchill and N. Lior, Numerical calculations of laminar and turbulent natural convection in water in rectangular channels heated and cooled isothermally on the opposing vertical walls, *Int. J. Heat Mass Transfer* **28**(1), 125–138 (1985).
10. R. Cheesewright and S. Ziai, Distributions of temperature and local heat-transfer rate in turbulent natural convection in a large rectangular cavity, *Proceedings of International Heat Transfer Conference*, Vol. 4, pp. 1465–1470 (1986).
11. A. Abrous and A. F. Emery, Turbulent free convection in square cavities with mixed boundary conditions, *Proceedings of National Heat Transfer Conference*, HTD-Vol. 107, pp. 117–131 (1989).
12. P. W. Giel and F. W. Schmidt, A comparison of turbulence modeling predictions to experimental measurements for high Rayleigh number natural convection in enclosures, *Proceedings of International Heat Transfer Conferences*, Vol. 2, pp. 175–181 (1990).
13. E. Nobile, A. C. M. Sousa and G. S. Barozzi, Turbulent buoyant flows in enclosures, *Proceedings of International Heat Transfer Conference*, Vol. 2, pp. 543–548 (1990).
14. T. G. Karayiannis, M. Ciofalo and G. Barbaro, On natural convection in a single and two zone rectangular enclosure, *Int. J. Heat Mass Transfer* **35**(7), 1645–1657 (1992).
15. F. G. Hammit, Natural-convection heat transfer in closed vessels with internal heat sources—analytical and experimental study, ASME Paper, 58-A212 (1958).
16. P. Essam, Free convection of heat generating fluids in cylindrical tanks, *Nucl. Engng. Design* **11**, 57–68 (1969).
17. W. Murgatroyd and A. Watson, An experimental investigation of the natural convection of a heat generating fluid within a closed vertical cylinder, *J. Mech. Engng Sci.* **12**(5), 354–363 (1970).
18. R. J. Kee, C. S. Landram and J. C. Miles, Natural convection of a heat-generating fluid within closed vertical cylinders and spheres, *J. Heat Transfer*, 55–61 (1976).
19. G. Fieg, Wärmeübergangsmessungen aus intern beheizten Flüssigkeiten in zylinderförmigen Konvektionszellen, KFK 2712, pp. 1–28 (1978).
20. N. K. Lambha, S. A. Korpela and F. A. Kulacki, Thermal convection in a cylindrical cavity with uniform volumetric energy generation, *Proceedings of International Heat Transfer Conference*, Vol. 2, pp. 311–316 (1978).
21. Y. S. Lin and R. G. Akins, Pseudo-steady-state natural convection heat transfer inside a vertical cylinder, *J. Heat Transfer* **108**, 310 (1986).
22. W. Smith and F. G. Hamitt, Natural convection in a rectangular cavity with internal heat generation, *Nucl. Sci Engng* **25**, 328–342 (1966).
23. U. Steinberner and H. H. Reinecke, Turbulent buoyancy convection heat transfer with internal heat sources, *Proceedings of International Heat Transfer Conference*, Vol. 2, pp. 305–310 (1978).
24. R. I. Bergholz, Natural convection of a heat generating fluid in a closed cavity, *Trans. ASME* **102**, 242–247 (1980).
25. G. A. Greene, T. F. Irvine, Jr and O. C. Jones, Jr, Experimental and analytical study of natural convection heat transfer of internally heated fluids, *Proceedings of International Heat Transfer Conference*, Vol. 2, pp. 135–140 (1982).
26. F. A. Kulacki and D. E. Richards, Natural convection in plane layers and cavities with volumetric energy sources, In *Natural Convection Fundamentals and Applications*, (Edited by: S. Kakaç, W. Aung and R. Viskanta), pp. 179–255 Hemisphere, Washington (1985).
27. J. H. Lee and R. J. Goldstein, An experimental study on natural convection heat transfer in an inclined square enclosure containing internal energy sources, *J. Heat Transfer* **110**, 345–349 (1988).
28. D. A. Kaminski and C. Prakash, Conjugate natural convection in a square enclosure: effect of conduction in one of the vertical walls, *Int. J. Heat Mass Transfer* **29**(12), 1979–1988 (1986).
29. D. B. Spalding, Mathematical modelling of fluid-mechanics, heat-transfer and chemical-reaction processes, A Lecture Course. Imperial College of Science and Technology CFDU Report, HTS/80/1 (1980).
30. M. Holzbecher, Ph.D., University of Dortmund, in preparation.

31. J. A. C. Humphrey and W. M. To, Numerical simulation of buoyant, turbulent flow—II Free and mixed convection in a heated cavity, *Int. J. Heat Mass Transfer* **29**(4), 593–610 (1986).
32. N. Z. Ince and B. E. Launder, On the computation of buoyancy-driven turbulent flows in rectangular enclosures, *Int. J. Heat Fluid Flow* **10**(2), 110–117 (1989).
33. L. Davidson, Calculation of the turbulent buoyancy-driven flow in a rectangular cavity using an efficient solver and two different low Reynolds number k–ε turbulence models, *Numer. Heat Transfer A* **18**, 129–147 (1990).
34. K. Hanjalic and S. Vasic, Numerical simulation of free convection in single- and multiple-zone rectangular cavities, *Proceedings of International Heat Transfer Conference*, Vol. 2, pp. 579–584 (1990).
35. R. A. W. M. Henkes, F. F. Van der Vlugt and C. J. Hoogendoorn, Natural-convection flow in a square cavity calculated with low-Reynolds-number turbulence models, *Int. J. Heat Mass Transfer* **34**(2), 377–388 (1991).
36. O. A. Plumb and L. A. Kennedy, Application of a k–ε turbulence model to natural convection from a vertical isothermal surface, *J. Heat Transfer* **99**, 79–85 (1977).
37. R. A. W. M. Henkes and C. J. Hoogendoorn, Comparison of turbulence models for the natural convection boundary layer along a heated vertical plate, *Int. J. Heat Mass Transfer* **32**(1), 157–169 (1989).
38. W. P. Jones and B. E. Launder, The calculation of low-Reynolds-number phenomena with a two-equation model of turbulence, *Int. J. Heat Mass Transfer* **16**, 1119–1130 (1973).
39. C. K. G. Lam and K. Bremhorst, A modified form of the k–ε model for predicting wall turbulence, *J Fluids Engng* **103**, 456–460 (1981).
40. K. Y. Chien, Predictions of channel and boundary-layer flows with a low-Reynolds-number turbulence model, *AIAA J.* **20**, 33–38 (1982).
41. K. Abe, T. Kondoh, and Y. Nagano, A new turbulence model for predicting fluid flow and heat transfer in separating and reattaching flows—I. Flow field calculations, *Int. J. Heat Mass Transfer* **37**, 139–151 (1994).
42. B. E. Launder and B. I. Sharma, Application of the energy-dissipation model of turbulence to the calculation of flow near a spinning disc, *Lett. Heat Mass Transfer* **1**, 131–138 (1974).
43. V. C. Patel, W. Rodi and G. Scheuerer, Turbulence models for near-wall and low Reynolds number flows. A review, *AIAA J.* **23**(9), 1308–1319 (1984).
44. R. A. W. M. Henkes and C. J. Hoogendorn, On the stability of the natural convection flow in a square cavity heated from the side, *Appl. Sci. Res.* **47**, 195–220 (1990).